

Journal of Materials Chemistry A

Accepted Manuscript



This is an *Accepted Manuscript*, which has been through the Royal Society of Chemistry peer review process and has been accepted for publication.

Accepted Manuscripts are published online shortly after acceptance, before technical editing, formatting and proof reading. Using this free service, authors can make their results available to the community, in citable form, before we publish the edited article. We will replace this *Accepted Manuscript* with the edited and formatted *Advance Article* as soon as it is available.

You can find more information about *Accepted Manuscripts* in the [Information for Authors](#).

Please note that technical editing may introduce minor changes to the text and/or graphics, which may alter content. The journal's standard [Terms & Conditions](#) and the [Ethical guidelines](#) still apply. In no event shall the Royal Society of Chemistry be held responsible for any errors or omissions in this *Accepted Manuscript* or any consequences arising from the use of any information it contains.

New versatile Pt supports composed of graphene sheets decorated by Fe₂O₃ nanorods and N-dopants with high activity based on improved metal/supports interaction

Yunqian Dai,^{1,*} Yunling Chai,¹ Yibai Sun,¹ Wanlin Fu,¹ Xiaotian Wang,¹ Qing Gu,¹
Tingying Helen Zeng² and Yueming Sun^{1,*}

¹*School of Chemistry and Chemical Engineering, Southeast University, Nanjing, Jiangsu 211189, P. R. China*

²*Center for Excitonics, Research Laboratory for Electronics, Massachusetts Institute of Technology, Cambridge, Massachusetts 02139, USA*

* Corresponding author: daiy@seu.edu.cn and sun@seu.edu.cn

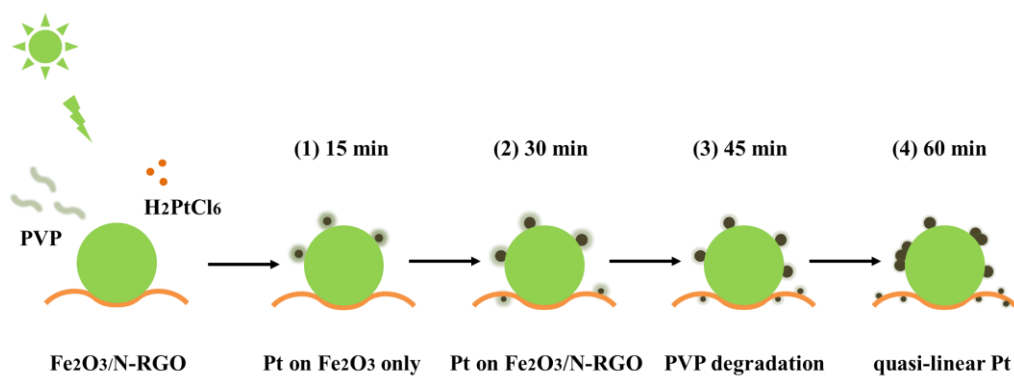
Abstract

Supported metal catalysts are critical to many important chemical reactions, but the weak metal/support interaction is an obstacle on the success of remarkable catalytic performance. This paper reports a rational-designed novel Pt supports, consisting of reduced graphene oxide sheets decorated with both Fe₂O₃ nanorods and N-dopants (denoted as Fe₂O₃/N-RGO), for Pt photodeposition driven by visible light in a controllable fashion. The 2-3 nm Pt nanocrystals primarily nucleated on rough Fe₂O₃ nanorods, and interacted strongly with special sites on Fe₂O₃ surface using unsaturated vacant orbitals. At the same time, the accelerated photodegradation of undesirable PVP allowed the Pt nanocrystals with clean active sites. The supported Pt showed impressive activity and had a 7-times higher reaction rate constant (11.4 s⁻¹ mg⁻¹) towards to 4-nitrophenol reduction, compared with that of free Pt, due to the synergetic effect within the whole Pt/Fe₂O₃/N-RGO catalysts and the doping of N atoms which acted as new metal-free catalytic centers in N-RGO sheets. We further demonstrated the ternary catalyst could be easily removed through a magnetic separation from system. This new strategy is extendible to other heterogeneous catalysts with different components.

Keywords: α -Fe₂O₃, graphene oxide, N-dopants, platinum

TOC

Improved catalytic performance was achieved when the well-designed $\text{Fe}_2\text{O}_3/\text{N-RGO}$ sheets served as a new and versatile scaffold for Pt nanocrystals, which exhibited a 7-times higher reaction rate constant.



Improved catalytic and photocatalytic performance is usually achieved in many important chemical reactions, when the catalysts are supported on specific substrates, mainly due to the change of electronic states in noble metals.¹ The remarkable activities of supported catalysts are greatly dependent on their chemical states, metal/support interactions, and their sizes. Typically, the catalysts, such as Pt nanocrystals, are dispersed finely on the porous carbon or metal oxide support,² that has abundant active sites to interact with metals. As a new emergence in carbon family, the graphene conjugated with sp^2 -hybridized carbon domains has been widely explored as a new two-dimensional (2D) scaffold in catalytic sciences.³ Doping heteroatoms, such as electron-rich N atoms, in graphene and/or its derivations is a promising way of manipulation their intrinsic electronic features and thus better interaction with catalysts to achieve enhanced performance.⁴ From this perspective, several success of this strategy have been demonstrated but still limited in reactions related to electrocatalytic or photocatalytic scopes,^{4b-d} like oxygen reduction reaction (ORR), water splitting and organic pollutant degradations. But the metal/carbon interaction is still weak at interface, and thus is an obstacle on the success of impressive catalytic performance.

The metal oxide (*e.g.* Fe_2O_3 , TiO_2 , CeO_2 and ZrO_2) is another widely explored ideal substrate that has excellent physical and chemical stability, especially the unique thermal stability required in many important industrial reaction, in which the carbon-based supports may not participate. An important breakthrough has been recently achieved in utilizing FeO_x nanocrystallites as metal supports for anchoring active single Pt atoms in CO oxidation, due to a facile charge transfer from Pt to FeO_x at metal/metal oxide interfaces.⁵ Recent efforts on TiO_2 supported Pt nanocrystals have demonstrated their excellent sinter-resistant ability,^{2b, 6} but these pre-synthesized PVP-stabilized Pt nanocrystals only exhibited weaker activities,⁶ as the presence of PVP on the interface hindered a direct contact between the metal and metal oxide. Several studies have shown that the calcination is a simple way to efficiently remove the surfactants, but the metal nanocrystals dramatically aggregate and thus lose active sites in high temperatures.⁷ Therefore, building a closed metal/support interface with

strong interaction at ambient temperature through a green chemistry approach is highly demanded but remains a significant challenge.

Herein, we report that the Pt nanocrystals can be selectively *in-situ* photodeposited on a well-designed supports, consisting of reduced graphene oxide sheets decorated with both Fe₂O₃ nanorods and N-dopants (denoted as Fe₂O₃/N-RGO). The versatile Fe₂O₃/N-RGO sheets here offer three functions: *i*) new photocatalysts for the deposition of Pt atoms and the simultaneous photodecomposition of PVP surfactant driven by visible-light, thus allowing Pt nanocrystals to contact with supports directly, *ii*) new substrates for the growth of Pt nanocrystals with well-established Pt/support interactions at a closed interface, and *iii*) magnetic materials for the rapid separation of catalyst from reaction system. By using this strategy, we were able to achieve a 7-times higher reaction rates than that of free-Pt nanocrystals.

Fig. 1A shows a typical TEM image of the Fe₂O₃/N-RGO hierarchical sheets. The graphene oxide (GO) sheets were simultaneously functionalized with Fe₂O₃ nanorods and N-dopants, via a one-pot hydrothermal reaction in ammonia aqueous solution by mixing GO sheets and electrospun α -Fe₂O₃ nanofibers (Fig. S1). After reaction, the pristine Fe₂O₃ nanofibers in fact converted to nanorods, but these morphology changes had no impact on their application described here, as the Fe₂O₃ nanorods maintained their highly irregular and rough surface, which can serve as primary nucleation sites for catalyst growth.⁸ Interestingly, we also observed nanopores (highlighted by black arrows in Fig. 1A) in a size of ~3 nm evenly dispersed in entire sheets, and the N-RGO sheets became holey. These nanosized holes are able to transport ions and molecules, and allow the graphene permeable for water desalination, gas separation, and DNA sequencing.⁹ Herein, they will also benefit the molecular migration during catalytic reaction. The N *1s* XPS spectrum in Fig. 1B could be deconvoluted into three peaks for pyridinic N (398.6 eV), predominant pyrrolic N (399.9 eV), and graphitic N (401.6 eV).¹⁰ Their atomic ratios to the total N *1s* atoms are calculated to be 0.33, 0.60, 0.065, respectively. No peak in the N *1s* spectrum could be assigned to the Fe-N bonding, suggesting the N-dopants most

likely bonded with C atoms selectively and thus had a very high N/C ratio up to 14.9 at% in N-RGO sheets, compared with elsewhere observed N-RGOs recently.¹¹ These N-dopants in graphene could enhance visible activities of Fe₂O₃ nanocrystallines greatly by improving the charge separation.^{4a} Therefore, the Fe₂O₃/N-RGO sheets are expected to have good performance in visible-light driven photocatalytic reaction and photovoltaic devices.

The Fe₂O₃/N-RGO sheets were demonstrated as a new substrates for a facile photodeposition of Pt nanocrystals driven by visible-light (>420 nm) in a controllable fashion. The evolution of Pt nanocrystals was investigated as a function of irradiation time, as shown in Fig. 2. After 15 min, a number of Pt nanocrystals with a size of 2.1 nm discretely and evenly dispersed on each Fe₂O₃ nanorods (Fig. 2A). The Fe₂O₃ nanorods acted as both a photocatalyst and a robust substrate for the growth of Pt nanocrystals. Interestingly, the Pt nanocrystals were rarely observed on the surface of N-RGO sheets, showing their favor of the rough Fe₂O₃ surface, as depicted in the inset of Fig. 2A. The irregularities on Fe₂O₃ surface, such as indentions, step edges, protrusions, or defective sites, significantly lowered the energy barrier for heterogeneous nucleation,⁸ and thus functioned as primary nucleation sites for the photodeposition of Pt atoms. And the selective deposition of Pt on Fe₂O₃ nanorods also confirmed the Fe₂O₃ interacted strongly with late transition metal. When the irradiation time was prolonged to 30 min, several tiny Pt nanocrystals appeared on the N-RGO sheets with a size of sub-2 nm, as indicated by black arrow in Fig. 2B, while the Pt on Fe₂O₃ nanorods had a bigger size of 2.4 nm and a higher density. Further prolonging the irradiation time to 45 min, the densities and sizes of Pt nanocrystals further increased on both Fe₂O₃ nanorods and the N-RGO sheets in Fig. 2C. These results clearly show that our photodeposition approach provides a superb control over the formation and distribution of Pt nanocrystals on the Fe₂O₃/N-RGO surface. These supports provide a large number of active sites for Pt nucleation which were evenly distributed over the entire surface, and thus ensured the generation of Pt nanocrystals without observed overlap between them. However, further prolonging the irradiation time to 60 min, a few of quasi-linear Pt agglomerations (highlighted by black ellipses

in Fig. 2D) appeared on Fe_2O_3 surface only, which were in fact composed of smaller nanocrystals loosely bonded together.¹² These linear-like Pt agglomerations had random orientation, which did not exhibit any preference in direction. In a contrast, the Pt nanocrystal on N-RGO sheets still kept their individuality well and had smaller sizes and lower coverages. Therefore the growth rates of Pt at different supports were different, and more than 90% of Pt nanocrystals were selectively deposited on the Fe_2O_3 nanorods. As shown in the HRTEM image (Fig. 2E), two truncated octahedron supported on the N-RGO sheets, and the lattice distance of 2.3 Å and 1.9 Å were the {111} and {200} facets of Pt nanocrystals.⁶ The inset in Fig. 2E illustrates a truncated octahedron supported on the N-RGO sheets. The nanopores on N-RGO sheets are less observable, which most likely have served as the favorable nucleation sites for Pt deposition. The Pt loadings were proportional with irradiation time (Fig. 2F), and the success of Pt growth at a low loading fashion (<2 wt%) is beneficial for decreasing noble metal consumption in a cost-saving mode.

Fig. 3A shows the Pt 4f XPS spectra of ternary Pt/ Fe_2O_3 /N-RGO catalysts, two predominant peaks centered at 75.6 eV and 72.2 eV belongs to the Pt 4f_{5/2} and Pt 4f_{7/2}, respectively. The Pt 4f_{7/2} had a ~1.0 eV up-shift, compared with the characteristic of metallic Pt⁰ (~71.2 eV).¹² This shift was assigned to the electron-deficient Pt^{δ+} state ((0<δ<2),^{8b} which indicated anchored Pt nanocrystals had unsaturated vacant orbitals possibly resulted from the transferring of their 5d electrons to the Fe_2O_3 nanorods,^{1c,5} and thus interacted strongly with special sites on supports. These low-coordination atoms on metal surface often act as excellent active sites, and are highly desirable in catalytic reactions. It can thus be concluded that the metallic Pt nanocrystals have been efficiently reduced by using Fe_2O_3 /N-RGO sheets as photocatalysts, and the metal/supports interactions also have been well-established that may play a vital role in anchor catalysts and enhance the remarkable catalytic activity. Bonding analysis of N 1s atoms (Fig. 3B and C) shows the N atoms had a predominant pyrrolic configuration and the N atomic ratio was directly proportional to the irradiation time. The increase in N at% implied the PVP, which contained pyrrolic N, gradually adsorbed on the Pt and/or the Fe_2O_3 /N-RGO surface. But the PVP, particularly those

on the Pt surface, encapsulate the Pt surface via the carbonyl bonds like a nanocage and thus are not favorable for the catalytic reactions.¹² We calculated the peak area ratio of pyrrolic N dopants to all N *1s* atoms (referred as $A_{\text{pyrrolic N}}/A_{\text{N1s}}$) for a simple comparison, on the basis of a hypothesis that the N-dopants in N-RGO sheets preserved their pristine bonding structures under irradiation. Thus the increase of $A_{\text{pyrrolic N}}/A_{\text{N1s}}$ ratio could be a facile indicator of the adsorption of PVP also. Surprisingly, the $A_{\text{pyrrolic N}}/A_{\text{N1s}}$ ratio decreased when more PVP were adsorbed as implied by a higher N at%, and was anti-proportional to the irradiation time after 45 min. This tendency uncovered the pyrrolic N structures were disrupted in PVP, and their degradation rate became faster than their adsorption rate. It has been reported the Fe_2O_3 have superiorly ability for photodegradation of many organic molecules especially when decorated with metal nanocrystals even at a level, and the metal surface are often the active centers for photocatalytic reaction.^{4a, 8b, 13} Therefore it is rational for us to deduce the Pt/ Fe_2O_3 /N-RGO hybrids have plenty of active sites for the photodegradation of PVP, particularly at the Pt surfaces, and the degradation rate of PVP on Pt is possibly faster than those on Fe_2O_3 /N-RGO. Moreover, the removal of PVP is also confirmed by the appearance of several loosely packed Pt structures in TEM analysis (Fig. 2D). Herein, the PVP had been selectively and partially removed, thus the Pt nanoparticles exposed more desired clean active sites for catalytic reaction.

We chose the reduction of 4-nitrophenol to 4-aminophenol by NaBH_4 as a model reaction to quantitatively evaluate their catalytic performances. This model reaction has a pseudo-first-order kinetics respected to the 4-nitrophenol (or 4-nitrophenolate).¹⁴ After adding the Pt/ Fe_2O_3 /N-RGO catalyst, a new peak at 315 nm for 4-aminophenol appeared, and the intensity of adsorption peak for 4-nitrophenol at 400 nm gradually dropped in a deceleration fashion, as the catalytic reaction processed (Fig. 4A). The kinetic process of the catalytic reduction could be conventionally monitored by measuring the normalized extinction at 400 nm as a function of time (Fig. 4B). We then use previously defined rate constant k_1 ,¹⁵ a normalized apparent rate constant (k_{app}) by mass (defined as $k_1=k_{\text{app}}/m$, where m is the weight of catalyst) to exclude the influence of catalyst mass on the reaction rate. Therefore, the k_1 reflects the intrinsic

catalytic activity. As shown in Fig. 4C, the free PVP-stabilized Pt nanoparticles (2.9 nm, Fig. S2) had a lowest k_1 value of $1.83 \text{ s}^{-1} \text{ mg}^{-1}$ similar to other reports.⁶ In a contrast, the supported Pt had a high k_1 , up to 7-times higher ($11.4 \text{ s}^{-1} \text{ mg}^{-1}$) than that of free Pt. And this impressive activity is advancing among other building blocks for Pt-based catalysts anchored on specific supports with different components consisting of metal oxides and/or graphene sheets recently (see Table S1).^{6, 14b-d} The unexpected, surprisingly better catalytic performances of our supported Pt could be mainly ascribed to the partially vacant $5d$ orbital of Pt atoms, less residual PVP on Pt surface, and strong Pt/supports interaction by which the Pt/Fe₂O₃ interface may serve as the primary active sites for the activation of 4-nitrophenol.^{1c} Surprisingly, we observed the Fe₂O₃/N-RGO sheets were in fact catalytically active towards to the reduction of 4-nitrophenol to 4-aminophenol despite of a weak activity without any Pt (Fig. S3A). To have a deeper insight of this unusual Pt-free catalytic activity, we evaluated the activity of N-RGO sheets and the Fe₂O₃ nanorods respectively, and found only the N-RGO sheets exhibited detectable activity to this reaction (Fig. S3B and C). Without the N-RGO sheets, the Pt/Fe₂O₃ nanorods, fabricated by the similar approach to the one for making the Pt/Fe₂O₃/N-RGO in Fig. 2C, only had a smaller k_1 of $7.98 \text{ s}^{-1} \text{ mg}^{-1}$ (Fig. S4). Such weaker activity indicated the versatile N-RGO sheets in fact acted as a new metal-free catalyst besides an ideal metal support, and had played a vital role on achieving the excellent catalytic performance of the ternary Pt/Fe₂O₃/N-RGO catalysts. The N-dopants in N-RGO sheets were believed to facilitate the adsorption and activation of 4-nitrophenol, and the carbon atoms bonded to them also became the active sites for reaction,¹⁵ and were responsible to our observed catalyst activity. Moreover, the synergistic effect between the N-dopants and the Pt on N-RGO sheets is also beneficial to a superior performance in this well-designed catalyst system. The turnover frequency (TOF) is another important indicator in the evaluation of catalytic efficiency. The approximate TOF that expressed as $([4\text{-nitrophenol}] \times \text{conversion}) / ([\text{Pt}] \times t)$ when the conversion reaches 90%, is calculated to be as high as $\sim 646 \text{ h}^{-1}$, indicating its good catalytic performance.^{3c, 14c} It is worth noting that, the Pt/Fe₂O₃/N-RGO sheets maintained a high stability over the course of

another five cycles of reactions (Fig. S5), exhibiting a good resistance against losing of activity due to Pt aggregation. Generally, the positively charged reaction product (4-aminophenol) could easily adsorb on PVP-stabilized Pt surface that have a negative charge, and thus causes poisoning of catalysts.^{14b, 16} Therefore, our observed good recyclability also uncovered the purified Pt had excellent stability against the poisoning, thanks to the efficient degradation of PVP.

The performances of supported Pt nanocrystals were strongly depended on their irradiation time in photodepositions, during which their sizes gradually increased from 2.1 nm to 3.1 nm. The k_1 increased with longer irradiation time and reached to the maximums of $11.4 \text{ s}^{-1} \text{ mg}^{-1}$ at 45 min. This tendency is consistent with the gradually degradation PVP on Pt surface under irradiation, and demonstrates the clean surface have more active sites. These cleaner surfaces in an increased proportion could promote the total activity towards the reaction in despite of bigger sizes. The k_1 value only slightly decreased to $10.7 \text{ s}^{-1} \text{ mg}^{-1}$ at 60 min, due to the formation of quasi-linear Pt agglomerations. Thus, the chemical state of exposed Pt species is of great importance in determining the activity of Pt/Fe₂O₃/N-RGO ternary catalysts.

As an important precursor, the α -Fe₂O₃ can also be conventionally converted into magnetic materials, such as magnetite (Fe₃O₄) by a simple reduction. In an effort to easily separate catalysts from reaction system, we simply reduced the Fe₂O₃ nanorods after finishing catalytic reaction, by adding the NaNH₄ into the solution system.¹⁷ The ternary catalysts exhibited rapid response to an external magnetic field (inset in Fig. 4D), that allowed a facile and rapid separation. These observations allow us to deduce the desired conversion of Fe₂O₃ to Fe₃O₄. And this hypothesis was then confirmed by the dramatically increased saturation magnetization (M_s) of 28.1 emu/g, from 2.5 emu/g of pristine Fe₂O₃/N-RGO sheets at room temperature.

In summary, a new rational-designed Pt-based ternary catalyst system with significantly improved activity was achieved by a green chemistry approach. In such system, the Fe₂O₃/N-RGO sheets showed versatile functions as visible active photocatalyst, ideal metal supports and magnetic materials. The supported 2-3 nm Pt nanoparticles exhibited an unexpected 7-times enhanced reaction rate up to 11.4

$\text{s}^{-1} \text{mg}^{-1}$, owing to the advantages brought by the well-established metal/support interaction during *in-situ* photodeposition, big portion of exposed clean surface, metal-free catalytic abilities arose from N-dopants, and the synergetic effect within the whole Pt/Fe₂O₃/N-RGO catalysts. The success of the strategy demonstrated may provide some inspirations that the utility of strongly interacted catalyst could open up a brand new approach to advanced heterogeneous catalysts with enhanced performances.

Acknowledgments

This work was financially supported by the National Basic Research Program (973 program, 2013CB932902), the National Natural Science Foundation of China (21201034, 21173042, 21310102005 and 21345008), the Science and Technology Support Program (Industry) Project of Jiangsu Province (BE 2013118) and the Fundamental Research Funds for the Central Universities (3207044403). T. Z. acknowledges funding from MIT Energy Initiative (MITEI) through MITEI-Weatherford International Corporation (Grant No. 6925033) and the MITEI seed funding (Grant No. 6925587) and Center for Excitonics at Massachusetts Institute of Technology, an Energy Frontier Research Center funded by the U.S. Department of Energy, Office of Science, and Office of Basic Energy Sciences under Award Number DE-SC0001088.

References

- 1 (a) C. T. Campbell, *Nature Chem.*, 2012, **4**, 597; (b) Y. Li and G. A. Somorjai, *Nano Lett.*, 2010, **10**, 2289; (c) N. An, S. Li, P. N. Duchesne, P. Wu, W. Zhang, J. Lee, S. Cheng, P. Zhang, M. Jia and W. Zhang, *J. Phys. Chem. C*, 2013, **117**, 21254; (d) S. Bai, J. Ge, L. Wang, M. Gong, M. Deng, Q. Kong, L. Song, J. Jiang, Q. Zhang, Y. Luo, Y. Xie and Y. Xiong, *Adv. Mater.*, 2014, **26**, 5689.
- 2 (a) P. Trogadas, T. F. Fuller, and P. Strasser, *Carbon*, 2014, **75**, 5; (b) Y. Dai, B. Lim, Y. Yang, C. M. Copley, W. Li, E. C. Cho, B. Grayson, P. T. Fanson, C. T. Campbell, Y. Sun and Y. Xia, *Angew. Chem. Int. Ed.*, 2010, **49**, 8165.
- 3 (a) Cheng Du, Yuxiang Liao, Xing Hua, Wei Luo, Shengli Chen and G. Chenga, *Chem. Comm.* 2014, **50**, 12843; (b) C. A. Tsang, K. N. Hui, K. S. Hui and L. Ren, *J. Mater. Chem. A*, 2014, **2**, 17986; (c) X. Lu, L. Yang, X. Bian, D. Chao and C. Wang, *Part. Part. Syst. Charact.*, 2014, **31**, 245; (d) S. Li, A. Wang, Y. Hu, K. Fang, J. Chen and J. Feng, *J. Mater. Chem. A*, 2014, **2**, 18177; (e) Q. Luo, X. Yu, B. Lei, H. Chen, D. Kuang, C. Su, *J. Phys. Chem. C* 2012, **116**, 8111-8117.
- 4 (a) L. Zhao, R. He, K. T. Rim, T. Schiros, K. S. Kim, H. Zhou, C. Gutiérrez, S. P. Chockalingam, C. J. Arguello, L. Pálová D. Nordlund, M. S. Hybertsen, D. R. Reichman, T. F. Heinz, P. Kim, A. Pinczuk, G. W. Flynn, and A. N. Pasupathy, *Science*, 2011, **333**, 999; (b) L. He, L. Jing, Y. Luan, L. Wang and H. Fu, *ACS Catal.* 2014, **4**, 990; (c) J. Zhu, M. Xiao, X. Zhao, K. Li, C. Liu and W. Xing, *Chem. Comm.* 2014, **50**, 12201-12203; (d) Y. Shao, S. Zhang, M. H. Engelhard, G. Li, G. Shao, Y. Wang, J. Liu, I. A. Aksay, and Y. Lin, *J. Mater. Chem.*, 2010, **20**, 7491.
- 5 B. Qiao, A. Wang, X. Yang, L. F. Allard, Z. Jiang, Y. Cui, J. Liu, J. Li and T. Zhang, *Nature Chem.*, 2011, **3**, 634.
- 6 (a) L. Ping, C. T. Campbell and Y. Xia, *Nano Lett.*, 2013, **13**, 4957; (b) L. Ping and Y. Xia, *ACS Appl. Mater. Interfaces*, 2013, **5**, 6391.
- 7 (a) L. Liu, S. Ouyang and J. Ye, *Angew. Chem. Int. Ed.*, 2013, **52**, 6689; (b) Z. Wang, H. Fu, D. Han and F. Gu, *J. Mater. Chem. A*, 2014, DOI: 10.1039/C4TA04524F.

- 8 (a) E. Formo, P. Camargo, B. Lim, M. Jiang and Y. Xia, *Chem. Phys. Lett.*, 2009, **476**, 56; (b) L. Chen, F. Li, B. Ni, J. Xu, Z. Fu and Y. Lu, *RSC Adv.*, 2012, **2**, 10057.
- 9 (a) D. Cohen-Tanugi and J. C. Grossman, *Nano Lett.*, 2012, **12**, 3602; (b) D. Jiang, V. R. Cooper and S. Dai, *Nano Lett.*, 2009, **9**, 4019.
- 10 Y. Dai, H. Long, X. Tian, Y. Wang, Q. Gu, W. Jiang, Y. Wang, C. Li, T. H. Zeng, Y. Sun and J. Zeng, *Part. Part. Syst. Character.*, 2014, **31**, 597.
- 11 H. Wang, T. Maiyalagan and X. Wang, *ACS Catal.*, 2012, **2**, 781.
- 12 Y. Borodko, P. Ercius, D. Zhrebetsky, Y. Wang, Y. Sun and G. Somorjai, *J. Phys. Chem. C*, 2013, **117**, 26667.
- 13 B. Xu, B. Huang, H. Cheng, Z. Wang, X. Qin, X. Zhang and Y. Dai, *Chem. Comm.*, 2012, **48**, 6529.
- 14 (a) R. He, Y. Wang, X. Wang, Z. Wang, G. Liu, W. Zhou, L. Wen, Q. Li, X. Wang, X. Chen, J. Zeng and J.G. Hou, *Nature Comm.*, 2014, **5**, 4327; (b) T. Yu, J. Zeng, B. Lim and Y. Xia, *Adv. Mater.*, 2010, **22**, 5188; (c) X. Wang, D. Liu, S. Song and H. Zhang, *J. Am. Chem. Soc.*, 2013, **135**, 15864; (d) Z. Ji, X. Shen, Y. Xu, G. Zhu and K. Chen, *J. Colloid Interface Sci.*, 2014, **432**, 57.
- 15 (a) X. Kong, Z. Sun, M. Chen, C. Chen and Q. Chen, *Energy Environ. Sci.*, 2013, **6**, 3260; (b) X. Kong, C. Chen and Q. Chen, *Chem. Soc. Rev.*, 2014, **43**, 2841.
- 16 H. Li, S. Gan, D. Han, W. Ma, B. Cai, W. Zhang, Q. Zhang and L. Niu, *J. Mater. Chem. A*, 2014, **2**, 3461.
- 17 F. Jiao, J. Jumas, M. Womes, A. V. Chadwick, A. Harrison and P. G. Bruce, *J. Am. Chem. Soc.*, 2006, **128**, 12905.

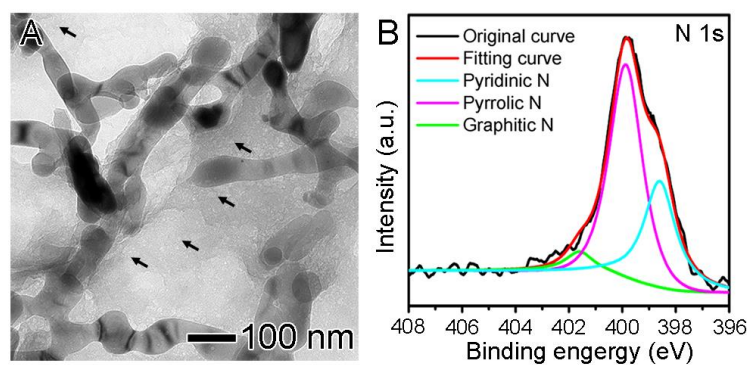


Figure 1. (A) TEM image of the Fe₂O₃/N-RGO sheets, obtained by hydrothermal treating a mixture of graphene oxide and Fe₂O₃ in 20 mL of ammonium hydroxide (1.9 mol/L). (B) N 1s high-resolution XPS spectrum of the sample in (A).

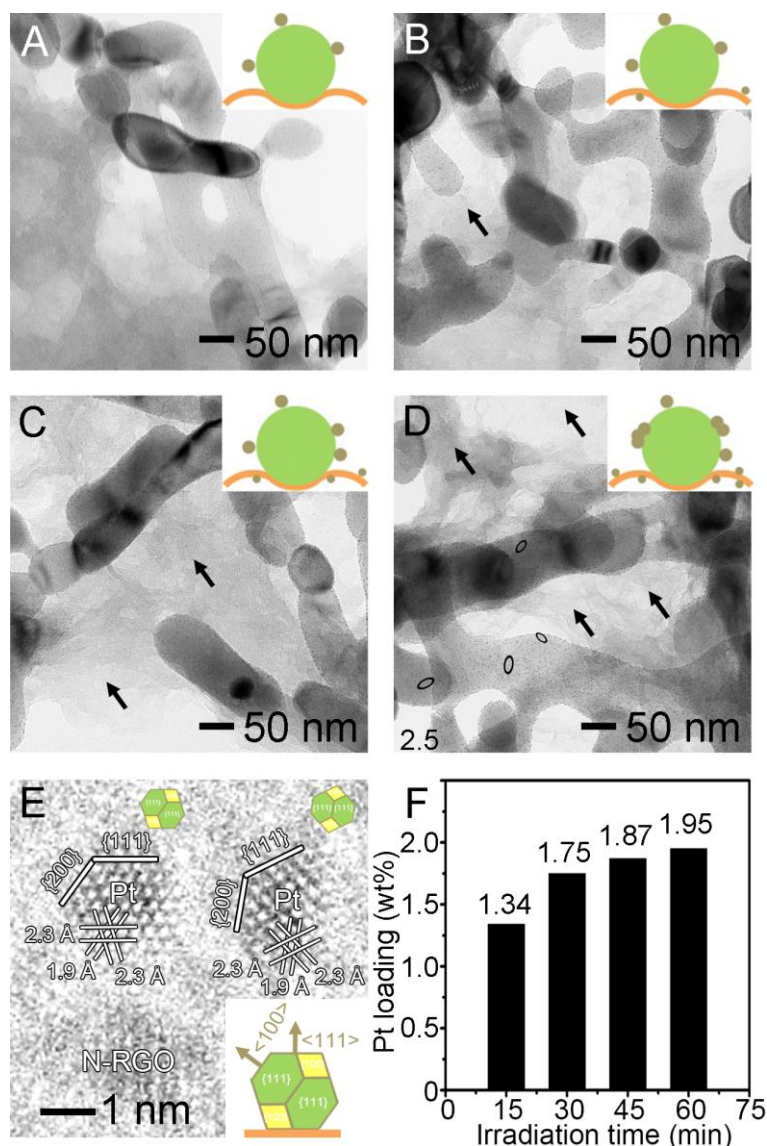


Figure 2. TEM images of the selective *in-situ* photodeposition of Pt nanocrystals on Fe₂O₃/N-RGO sheets under a visible light irradiation for (A) 15, (B) 30, (C) 45 and (D) 60 min, respectively. The insets in (A to D) depict the changes of size, density and morphology of Pt nanocrystals on the supports. The black arrows highlight several typical Pt nanoparticles on the N-RGO sheets, while the black ellipses in (D) highlight the quasi-linear aligned Pt nanocrystals on Fe₂O₃. (E) HRTEM image of the Pt supported on the N-RGO sheets, and the inset showing its schematic model. (F) The dependence of Pt loading (wt%) on the irradiation time.

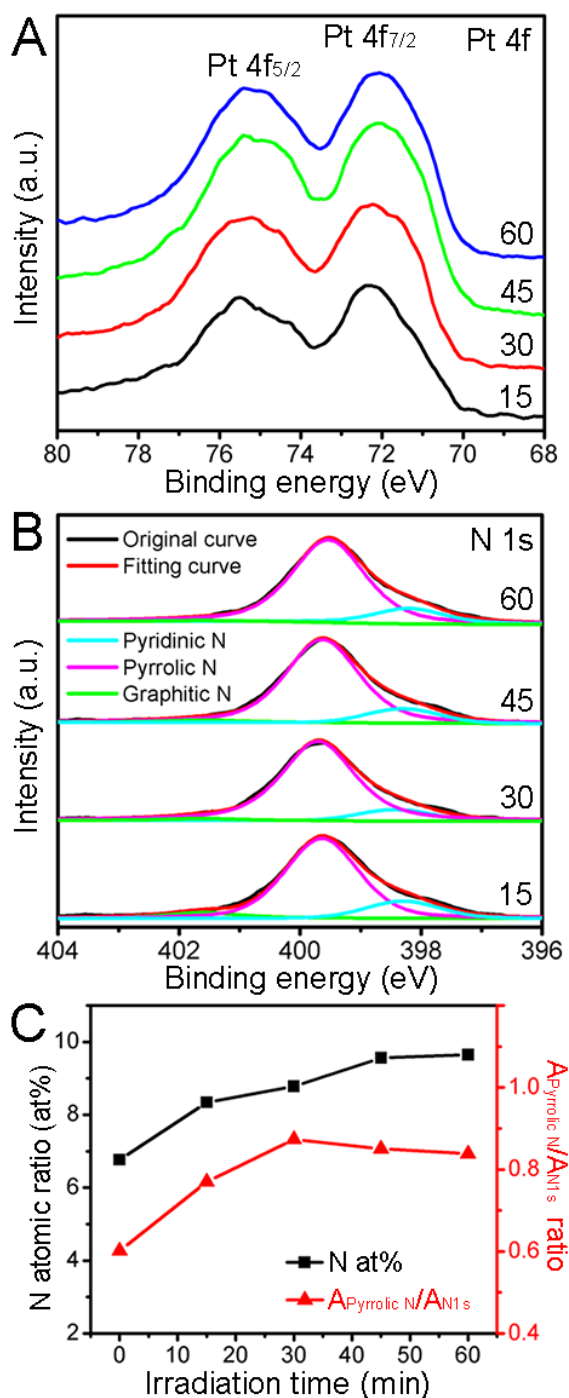


Figure 3. (A) Pt 4f and (B) N 1s high-resolution XPS spectra of the Pt/Fe₂O₃/N-RGO catalysts irradiated with varied times. (C) The plots showing the N atomic ratio and the peak area ratio of pyrrolic N to all N 1s (referred to as $A_{\text{pyrrolic N}}/A_{\text{N1s}}$) versus irradiation time.

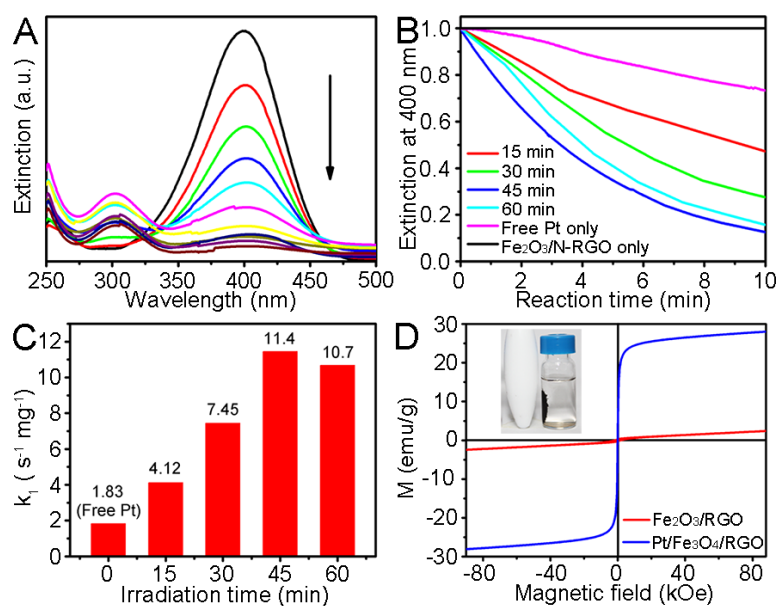


Figure 4. (A) A series of extinction spectra recorded at different reaction time, showing the proceeded reduction of 4-nitrophenol to 4-aminophenol. (B) The normalized extinction at 400 nm for the reaction system as a function of time after adding Pt/Fe₂O₃/N-RGO, free Pt and pristine Fe₂O₃/N-RGO sheets. (C) A plot of reaction rate (k_1) versus irradiation time, showing the supported Pt had a maximum 7-times higher k_1 than that of free Pt. (D) The room temperature hysteresis loops of the ternary catalyst after reduction (in blue) and the pristine Fe₂O₃/N-RGO sheets (in red). The inset photograph illustrates the magnetic separation of ternary catalyst in an external magnetic field.